A blind survey for molecular gas in a z = 2.84 proto-cluster of galaxies

Scott Chapman,[1*] Colin Ross,[1] Manuel Aravena,[2] Andrew Blain,[3] Jim Geach,[4] Mark Gurwell,[5] Rob Ivison,[6]Naveen Reddy,[7] Ian Smail,[8] Chuck Steidel[9]

[1]Department of Physics and Atmospheric Science, Dalhousie University, Coburg Road Halifax, B3H 4R2

[2]European Southern Observatory, Alonso de Córdoba 3107, Vitacura, Santiago, Chile,

[3]Physics and Astronomy, University of Leicester, University Road Leicester, LE1 7RH

[4]Department of Physics, Ernest Rutherford Building, 3600 rue University, McGill University, Montreal, QC, H3A 2T8, Canada

[5]Harvard CfA

[6]UK Astronomy Technology Centre, Royal Observatory, Blackford Hill, Edinburgh EH9 3HJ

[7]Department of Physics and Astronomy, UC Riverside, 900 University Avenue, Riverside, CA 92521

[8]Institute for Computational Cosmology, Department of Physics, Durham University, South Road, Durham DH1 3LE

[9]Cahill Center for Astronomy and Astrophysics, California Institute of Technology, MS 249-17, Pasadena, CA 91125, USA

*To whom correspondence should be addressed; E-mail: scott.chapman@dal.ca.

Measuring the evolution of molecular gas density is critical to understand the formation of molecular gas and stars in galaxies. However, the gas supplies, star formation efficiencies, and starburst modes (merger driven versus quiescent disk) may vary strongly as a function of their local density, and comparing the CO properties of galaxies in protoclusters to the field will elucidate the stronger evolution seen in overdense regions. In this letter, we describe a blind 3mm search for CO(3-2) molecular gas from $z \sim 2.8$ galaxies in the most overdense galaxy cluster known at z>2, from the Keck Baryonic Structure Survey (Rudie et al. 2012). The extremely strong clustering of galaxies in angular

scales and along the line of sight effectively increases the number of galaxies observed within a single pointing with the IRAM-PdBI. From the known ~ 22 PdBI-targeted galaxies in this structure and their SFRs, we expect to detect at most two CO line emitters, scaling from field galaxy studies. However, we find five CO lines with S/N>5 associated to known UV-bright protocluster galaxies, and as many as 8 $z \sim 2.84$ CO line emitters in total. This provides a solid constraint on the evolving CO luminosity function in overdense fields. The higher than expected fraction of galaxies with large CO gas masses tells us that this overdense region is in a process of forming stars at a tremendous rate. We compare gas/dynamical masses and the Millenium simulation to constrain how rare such structures are, finding that one is expected every $\sim$20 deg^2 on the sky. We also constrain our findings empirically using the lack of similar clustering in the CO surveys of Bothwell et al. (2013) and Tacconi et al. (2010), and Daddi et al. (2010), where no additional CO sources beyond the targeted source are found in the vicinity of >50 PdBI fields. The higher detectability rate is likely because the cluster galaxies are more biased, and hence more massive, than the field, as found from the large measured stellar masses of 4 of 6 of our CO emitters. This appears to be the gas equivalent of the reversal in the relation claimed at $z \sim 1.5 - 2$ for star formation and environment, with the cluster population having higher gas masses than the field.

Introduction

One of the major goals of modern observational cosmology is to understand how the gas in the diffuse interstellar medium (ISM) of galaxies converts into stars and how both phases evolve with cosmic time. A major advance has been the determination of the evolution of the SFR

density of the Universe. Deep optical and radio surveys indicated that the SFR density steadily increases from $z = 5$, with a peak at $z \sim 3 - 1$, and steeply declines from $z = 1$ to the present Lilly1996, Madau1996, Cowie1999, Steidel1999, Giavalisco2004, Ouchi2004, Bouwens2007, Smolcic2009. Although the contribution from luminous, merger-driven starburst galaxies at high-redshift to the SFR density appears to be significant, the population that drives such evolution appears to be formed by more quiescent massive star-forming galaxies Daddi2007, Rodighiero2011. The close relationship between the SFR and the amount of molecular gas in galaxies, from which stars form, suggest that the evolution of the SFR density is the result of the evolution of the molecular gas density in galaxies across cosmic times.

Measuring the evolution of this molecular gas density is thus critical to understand the formation of molecular gas and stars in galaxies. For this, it is necessary to perform blind surveys of the sky that allow us to measure the molecular gas content in a CO flux limited sample as a function of redshift and luminosity [e.g. observations in the local Universe and simulations by] Keres2003, Obreschkow2009a, Obreschkow2009b. The technical limitations (e.g. bandwidth, sensitivity) of current submillimeter and radio facilities, along with the intrinsic faintness of the CO emission lines used to measure the amount of molecular gas in galaxies have, however, precluded such studies.

Observations and Sample

We have obtained a deep PdBI pointing tuned to redshifted CO(3-2) in the 3mm band for the H1549, galaxy overdensity field (Steidel et al. 2005, 2010), depicted in Fig. 1. Because of its minimal excitation requirements, CO J=3-2 offers the best view of the mass/distribution of star forming gas in a range of galaxy types/luminosities. The extremely strong clustering of galaxies in angular scales and importantly along the line of sight, $\sim$2000 km/s line of sight depth for the FWHM of the galaxy N(z), makes it possible to effectively increase the number of galaxies

observed within the PdBI-WIDEX pointing.

The target field was chosen from the 24 survey fields of the Keck Baryonic Structure Survey (KBSS – e.g., Rudie et al. 2012). Several of these fields show strong galaxy overdensities (e.g., Steidel et al. 2000, 2005, 2010), and together represent a complete, unbiased census of overdensities in a well-calibrated field galaxy survey at $z > 2$. The H1549 field targeted in this study represents the strongest overdensity ($z\sim$2.84) found in the KBSS, and has $> 5\times$ the surface density of Lyman-alpha emitters (LAEs) compared to the average among ~ 20 fields covered to a similar depth, representing the richest field of Ly$alpha$-selected objects ever observed, at any redshift.

We have also observed this field with SCUBA2 at 850μm and 450μm down to a 1σ RMS of 0.8 mJy. The SCUBA2 map at 850μm is overlaid on the IRAC 4.5μm map in Fig. 1, where significantly detected CO(3-2) sources consistent with lying in the protocluster are highlighted.

We detect, at $> 5\sigma$ the CO $3-2$ emission line from five galaxies known to be at $z \sim 2.84$ with available spectroscopic redshifts (Table 1), an additional three known $z \sim 2.84$ galaxies at $> 3.5\sigma$, and one candidate $z \sim 2.84$ CO emitter with no known optical counterpart (C1 in Table 1). We find $L'_{\rm CO}$ ranges from $(3.9 \pm 1.1) \times 10^{10}$ K km s^{-1} pc^2 to $(1.3 \pm 0.4) \times 10^{10}$ K km s^{-1} pc^2. SCUBA2 detects at 850μm, an unresolved complex of emission encompassing 4 of the strongest CO line emitters in this structure, with 450μm emission detected over the central two sources. These galaxies are also detected with *Spitzer* at 24 μm. The CO detected galaxies are shown individually in Fig. 2.

Results

Constraints on optical-CO properties in a dense environment:

In Fig. 3 we show the predicted cosmic evolution of the space density of CO emitting galaxies as a function of CO luminosity (CO luminosity function) at redshifts z = 0–2. Our CO

survey of star forming galaxies in the H1549, H1700, and Q2345 clusters will add significantly to our understanding of the optical-CO properties and the gas fractions of star forming galaxies in overdense regions at $z\sim$2.5, characterizing the CO(3-2) of the higher gas mass range of galaxies individually, and the lower range of M_{H_2} on average (through stacking). Since the overdensities themselves are well characterised relative to the field, they will provide an important baseline for comparing with the field luminosity function that is emerging from other studies (e.g., Walter et al. 2012, Geach et al. 2012). The dense environment will likely bias the evolution of galaxies in the region differently than in the field – in fact we will be able to start to characterize the effect of the large overdensity on the gas supplies and star formation modes with our CO detections and stacked CO properties.

Through our blind survey of CO(3-2) gas in this field, we have begun to assess the importance and variation of gas supply to the reversal of the star formation-density relation at $z>2$ (e.g., Tran et al. 2011), understanding for the first time the star formation efficiencies leading to the exceptionally high levels of star formation found in our cluster cores. We use the sample of 40 CO-observed SMGs (Bothwell et al. 2012) and the census of CO(3-2) in normal z=1-2 star forming galaxies (Tacconi et al. 2010, Daddi et al., 2010) as a "field" comparison. CO emission is the standard probe of gas mass in these high-redshift galaxies, but suffers from uncertainties in CO -H_2 conversion (factor 4 difference between the Bothwell et al. SMGs and Tacconi et al. SF galaxies). A comparison of dynamical, stellar, and molecular gas masses in these galaxies will allow us to constrain the variation of CO-H_2 conversions across the protocluster population versus the field population (e.g., Genzel et al. 2012). We thus begin to calibrate the average SF-efficiencies in star forming galaxies in protoclusters versus the field.

Discussion

In this work, we have presented deep CO $3-2$ line observations of galaxies located in a galaxy cluster candidate at $z = 2.84$ using the IRAM PdBI. The candidate cluster was identified using the red-sequence technique and is associated to an overdensity of $\sim \times 10$ of star-forming galaxies. We use the spatial clustering and expanded bandwidth of the PdBI to simultaneously observe the CO emission from 22 galaxies with available optical spectroscopic redshifts in a single pointing and frequency setting.

We performed a blind search for significant ($> 3.5\sigma$) emission line peaks in the PdBI data cube around the position of optical sources that were selected to have spectroscopic redshift in the range $z = 2.74 - 2.86$ covered by our PdBI frequency band. We find 6 sources in the protocluster at $> 5\sigma$, and an additional 3 protocluster galaxies have detected CO line emission at lower signfiicance.

Chance probabilities and monte carlo experiment.

We find CO based spectroscopic redshifts compared to optical redshifts as listed in Table 1. The 24 μm and 850 μm with *Spitzer* and *JCMT* lead to IR luminosities ranging from $11.9 \times 10^{11}\ L_{\odot}$ to $3.3 \times 10^{11}\ L_{\odot}$. In 3 cases, optical/IR SED suggest a $\sim$1 Gyr old, very massive star forming galaxy, with a stellar mass of $1.1 \times 10^{11}\ M_{\odot}$, while for two others the SED indicates that it corresponds to a young star-forming galaxy, with a stellar mass of $2.8 \times 10^{10}\ M_{\odot}$. For the quasar host and the companion galaxy next to it, we are unable to accurately constrain the stellar emission.

We measured the space density of CO galaxies compared to the space density of CO emitters estimated from UV-selected galaxies with high SFRs from Tacconi et al. (2010), and the 6 BzK galaxies significantly detected in CO emission by Daddi et al. (2010), and compared to predictions from semi-analytic simulations. Overall, we find that all observations are only roughly

consistent with the simulations, despite the low number of detections of typical star-forming galaxies at high-redshift. Clearly, observations of molecular gas from a statistically significant sample of these galaxies is necessary to measure the evolution of CO luminosity function with redshift, and thus constrain models of galaxy formation and evolution. We conclude by discussing the advantages of performing deep CO observations of star-forming galaxies in clustered fields compared to blank-fields in the sky.

Conclusions

The determination of redshifts for galaxies based on (sub)millimeter and radio wavelength observations have been focused on the IR brightest sources, favored by the expanded bandwidth of such facilities. Based on the relationship between IR and CO luminosities, an IR bright galaxy, such as an SMG, is likely to also have bright CO emission. This facilitates a high significance "blind" CO emission line detection along the line of sight, leading to an accurate redshift measurement. In such studies, the position of their targets are known a priori, usually derived from large blank-field IR/submm surveys, permitting to spatially guide the CO observations, being thus not really "blind" CO detections

Blind spectroscopic imaging of the sky with large bandwidths have a huge potential for discovery of gas-rich, optically and IR faint galaxies, however they require deep integrations to ensure significant emission line detections, at the $\sim 10\sigma$ level, and unequivocally identify the galaxies and their redshifts. In the absence of such high signal-to-noise detections, observations need to be guided by well-known optical, IR or radio positions and by accurate photometric redshifts. As shown in this work, focused line observations of clustered fields at high-redshift have the advantage to increase the likelihood of finding gas emission using a limited bandwidth. This approach reduces the required observing time compared to purely blank fields, where besides the need to cover a substantial area of the sky, it is necessary either to cover a reasonable

range in frequency (e.g. a full 3 mm band for ALMA,in order to contain emission lines at different redshifts.

Fig. 1. Sources in the field of H1547 at different wavelengths. The white circle represents the location of the PdBI pointing and primary beam (PB) FWHM. Red contours show SCUBA2 850μm map at contours starting at 2σ spaced by 1σ. Background image is IRAC 4.5μm – the rest frame 1.6μm at $z = 2.84$. Blue circles show the CO(3-2) detections in Table 1, drawn at the size of the PdBI beam ($\sim 3''$). Projected number density of galaxies with $z_{\rm phot} = 2.80$–2.86 and SFR > 10 M$_\odot$ yr^{-1} in a $3' \times 3'$ region around the cluster center. Should show with grayscale and contours the density of galaxies in this field, δ_C, given in terms of the average density δ_0 of similarly selected galaxies in the h1549 field, $\delta = \delta_C/\delta_0$.

Fig. 2. CO(3-2) line detections ($> 5\sigma$) of five $z\sim$2.84 galaxies in the field. The first spectrum and channel map shows the two central sources which are blended together in the PdBI beam, but separate out by 2$''$ in the respective channel maps of the two sources. The other three CO sources are relatively isolated, although both D14 and NB63 may have contributions from more than one galaxy. Three other candidate CO detections are found at lower signficance (3.5-4.4σ). One further $> 5\sigma$ source is not identified with any known optical galaxies, the high significance of the CO detection suggests it may be very faint, obscured, starbursting systems in the protocluster. No other known galaxies are detected outside of the protocluster.

Fig. 3. Predicted (Obreschkow et al. 2009) cosmic evolution of the space density of CO emitting galaxies at redshifts z=0 (gray solid line, plus Keres et al. 2003 measurements), z=1 (black dashed line), z=3 (black solid line). Also shown, the space density of 2 CO detections from a JVLA pointing in the COSMOS field (black filled), the 6 BzK star-forming galaxies at z=1.5 (Daddi et al. 2010 – black open). Our PdBI observations will provide key constraints on the CO(3-2) luminosity distribution in well characterized, highly overdense regions, which can be compared with the field population.

References and Notes

1. Aravena M. et al., 2010, ApJ, 718, 177
2. Aravena M. et al., 2012, arXiv:1207.2795
3. Bothwell M., et al., 2012, arXiv1205.1511
4. Daddi E., et al. 2008, ApJ, 673, L21
5. Daddi E. et al., 2010, ApJ, 714, L118
6. Elbaz D., et al., 2007 A&A, 468,33
7. Elbaz D., et al., 2011 A&A, 533,119
8. Forster Schreiber et al. 2009, ApJ, 532, 133
10. Geach & Papadopoulos 2012, ApJ, arXiv1206.4693
11. Geach J. E., et al., 2011, ApJ, 730, L19
12. Genzel et al. 2012, ApJ, 746, 69
13. Greve T. R. et al., 2005, MNRAS, 359, 1165
14. Ivison R., et al., 2011,MNRAS.412.1913
15. Keres D., Yun M. S., Young J. S., 2003, ApJ, 582, 659
16. Lagos C. D. P., et al., 2011, MNRAS, 418, 1649
17. Obreschkow D., et al., 2009, ApJ, 702, 1321
18. Obreschkow D., Rawlings S., 2009, ApJ, 696, L129

Table 1: Main properties of CO-detected proto-cluster galaxies.

ID	RA / Dec	$S_{CO(3-2)}$ (Jy km/s)	S/N	L′(CO) ($L_\odot$)	σ(CO) (km/s)	z(UV)	z(CO)	co
Q1549	15:51:52.45 +19:11:03.8	0.778	12.4			2.844	2.847	QS
MD17	15:51:53.77 +19:11:09.7	0.528	10.8			2.845	2.856	3mm c
NB63	15:51:53.98 +19:10:41.8	0.505	6.4			2.843	2.841	A28-31, two m
Q1549nbr	15:51:52.57 +19:11:05.4	0.229	5.4			—	2.839	neighb
D14	15:51:53.21 +19:10:59.5	0.325	5.3			2.851	2.853	massiv
MD12	15:51:51.88 +19:10:41.2	0.553	4.5			2.851	2.847	massiv
M15	15:51:51.26 +19:11:05.6	0.247	4.2			2.849	2.853	
NB133	15:51:54.76 +19:11:06.3	0.215	4.0			2.844	2.847	
C1	15:51:50.80 +19:11:40.0	0.313	5.1			n/a	2.853	no known op

19. Riechers D., et al., 2010 ApJ, 724,153

20. Rudie G., et al., 2012 ApJ, 750,67

21. Steidel, C., et al 2011, ApJ, 736, 60

22. Steidel, C., Erb, D.K., Shapley, A.E., et al 2010, ApJ, 717, 289

23. Steidel, C., et al 2005, ApJ, 626, 44

24. Steidel, C., Adelberger, K., Shapley, A., et al. 2000, ApJ, 532, 170

25. Tacconi L. J. et al., 2010, Nature, 463, 781

26. Tran K.-V., et al., 2010, ApJ, 719L,126

27. Walter F., et al., 2012, Nature, 486 233

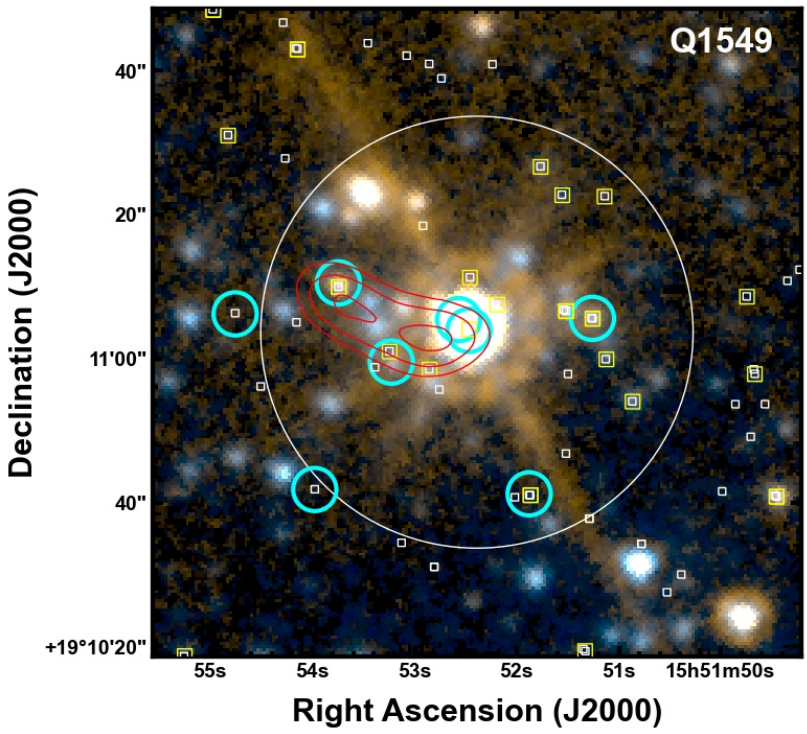
Q1549
40"
20"
11'00"
40"
+19°10'20"
55s
54s
53s
52s
51s
15h51m50s
Declination (J2000)
Right Ascension (J2000)

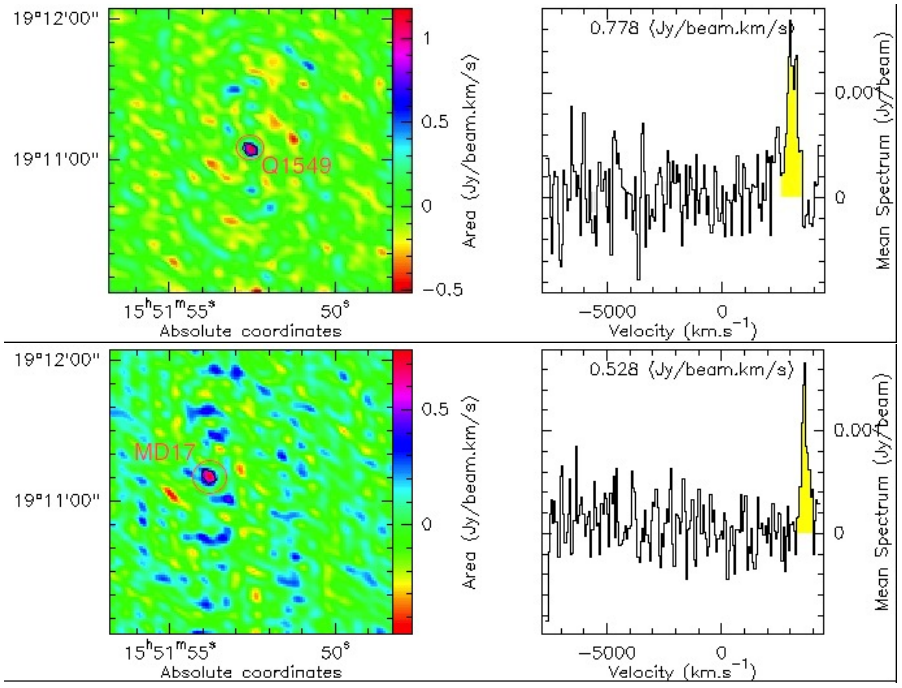
19°12'00"
19°11'00"
Q1549
1
0.5
0
−0.5
Area (Jy/beam.km/s)
15h51m55s
50s
Absolute coordinates
0.778 (Jy/beam.km/s)
0.001
0
Mean Spectrum (Jy/beam)
−5000
0
Velocity (km.s−1)
19°12'00"
19°11'00"
MD17
0.5
0
Area (Jy/beam.km/s)
15h51m55s
50s
Absolute coordinates
0.528 (Jy/beam.km/s)
0.001
0
Mean Spectrum (Jy/beam)
−5000
0
Velocity (km.s−1)

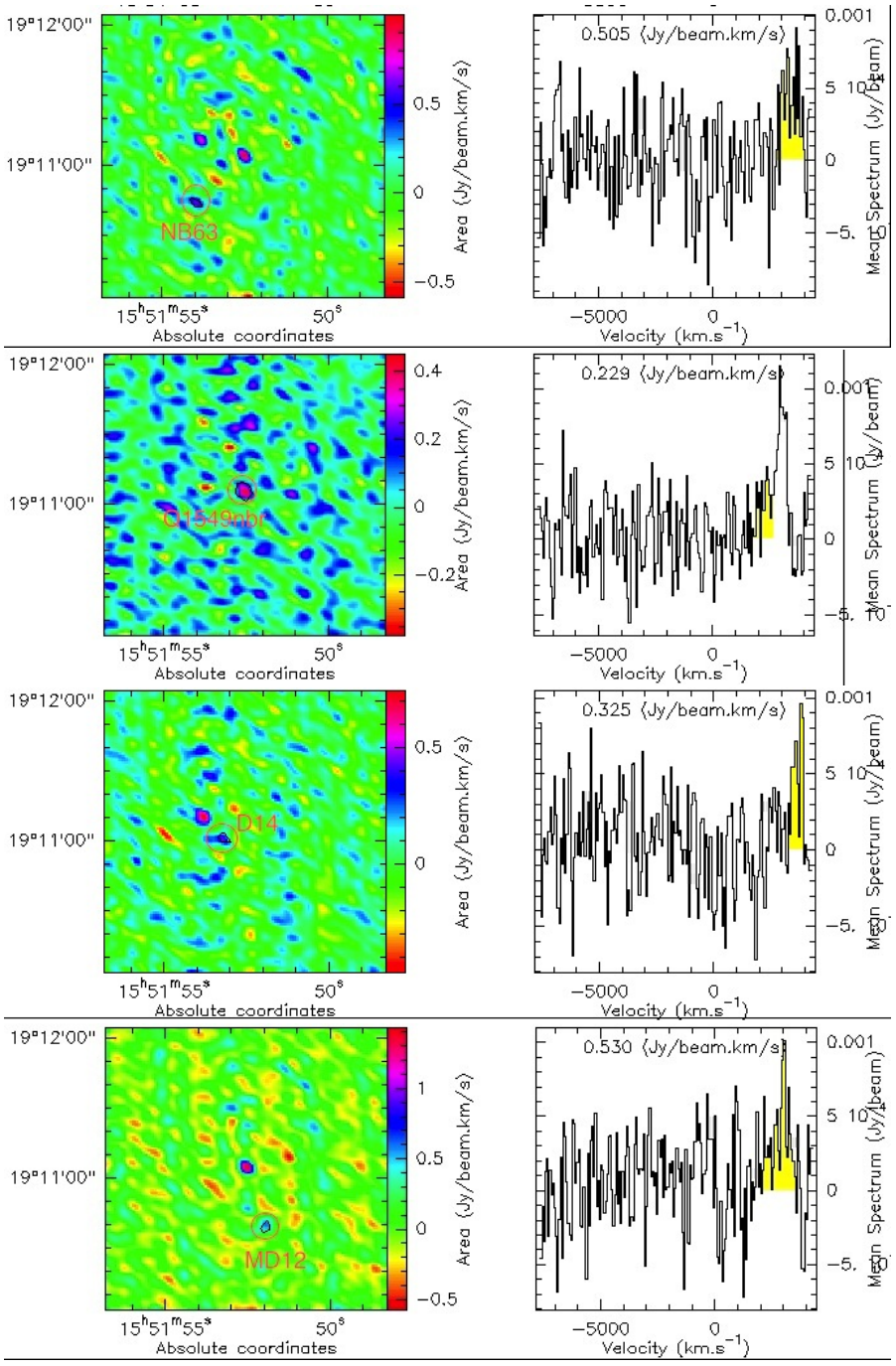
19°12'00"
19°11'00"
NB63
15h51m55s
50s
Absolute coordinates
Area (Jy/beam.km/s)
0.5
0
−0.5
0.505 (Jy/beam.km/s)
0.001
5 10−4
0
−5.
Mean Spectrum (Jy/beam)
−5000
0
Velocity (km.s−1)
19°12'00"
19°11'00"
C1549abf
0.4
0.2
0
−0.2
0.229 (Jy/beam.km/s)
19°12'00"
19°11'00"
D14
0.5
0
0.325 (Jy/beam.km/s)
19°12'00"
19°11'00"
MD12
1
0.5
0
−0.5
0.530 (Jy/beam.km/s)

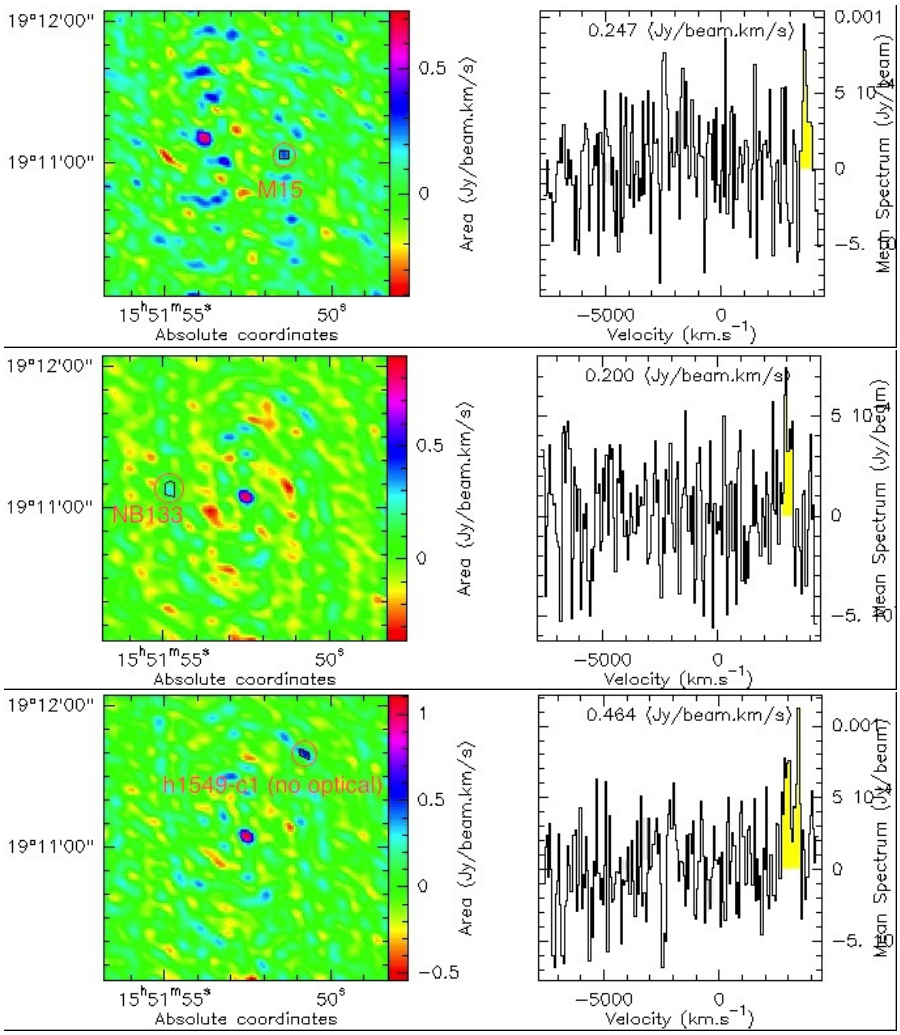
19°12'00"
19°11'00"
M15
15h51m55s
50s
Absolute coordinates
Area (Jy/beam.km/s)
0.5
0
0.247 (Jy/beam.km/s)
0.001
5 10-4
0
-5.
Mean Spectrum (Jy/beam)
-5000
0
Velocity (km.s-1)
19°12'00"
19°11'00"
NB133
15h51m55s
50s
Absolute coordinates
Area (Jy/beam.km/s)
0.5
0
0.200 (Jy/beam.km/s)
5 10-4
0
-5.
Mean Spectrum (Jy/beam)
-5000
0
Velocity (km.s-1)
19°12'00"
19°11'00"
h1549-c1 (no optical)
15h51m55s
50s
Absolute coordinates
Area (Jy/beam.km/s)
1
0.5
0
-0.5
0.464 (Jy/beam.km/s)
0.001
5 10-4
0
-5.
Mean Spectrum (Jy/beam)
-5000
0
Velocity (km.s-1)

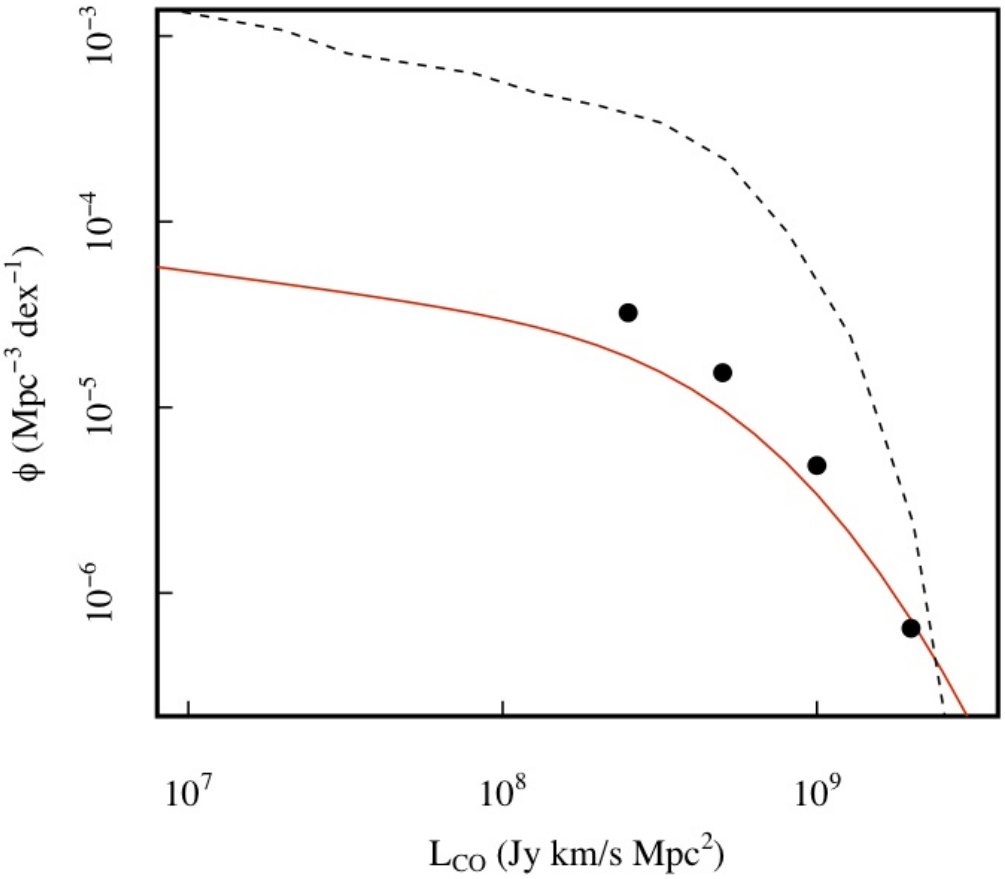
10^{-3}
10^{-4}
10^{-5}
10^{-6}
ϕ (Mpc^{-3} dex^{-1})
10^{7}
10^{8}
10^{9}
L_{CO} (Jy km/s Mpc^{2})

SUPPLEMENTAL MATERIAL

0.1 Line and continuum diagnostics

In Figs. A1-A3 we show the properties LCO, SFE, M* etc. Conclude XYZ - sumarized in text – see descriptions

0.2 Description of datasets

0.2.1 Details of the IRAM-PdBI observations

0.2.2 SCUBA2 data and reductions, 450um map.

Observations with the SCUBA2 camera on the JCMT were conducted in Band 2 weather conditions ($\tau_{225GHz} \sim 0.07$) over 4 nights between 4th April and 20th June 2012 totalling 6 hours of on-sky integration. The mapping centre of the SCUBA2 H1549 field is α = 15:51:52.47 +19:11:03.3, chosen as the apparent center of the galaxy over-density at $z = 2.85$ (Steidel et al. 2010). A standard 3 arcmin diameter 'daisy' mapping pattern was used, which keeps the pointing centre on one of the four SCUBA2 sub-arrays at all times during exposure.

Individual 30 min scans are reduced using the dynamic iterative map-maker of the SMURF package (Jenness et al. 2011; Chapin et al. 2012 in prep). Raw data are first flat-fielded using ramps bracketing every science observation. The map maker attempts to solve for noise and astronomical signal model components, refining a model until convergence is met, an acceptable tolerance has been reached, or a fixed number of iterations has been exhausted (in this case, 20). The signal from each bolometer's resulting data time stream is then re-gridded onto a map, according to the scan pattern, with the contribution to a given pixel weighted according to its time-domain variance. The sky opacity at JCMT has been obtained by fitting extinction models to hundreds of standard calibrators observed since the commissioning of SCUBA2 (Dempsey et al. 2012). The optical depth in the 850μm band was found to scale with the Caltech Submillimetre Observatory (CSO) 225 GHz optical depth.

Filtering of the time-series is performed in the frequency domain, with band-pass filters equivalent to angular scales of $2'' < \theta < 120''$ Spike removal ($> 10\sigma$ deviations in a moving boxcar), DC step corrections are also applied, and bad bolometers flagged. Maps from independent scans are co-added in an optimal stack using the variance of the data contributing to each pixel to weight spatially aligned pixels. A beam matched filter is then applied to improve point source detectability, resulting in a map that is convolved with an estimate of the 850μm beam. The average exposure time over the nominal 3 arcminute daisy mapping region is approximately 1000 sec per 2?? ? 2?? pixel.

A beam-matched flux conversion factor (FCF) has been derived from the subset of standard calibrators observed on the nights of the observations, FCF850 = 60$\pm$6 Jy beam^{-1} pW^{-1}. A correction of 10% is included in order to compensate for flux lost due to filtering in the blank-field map.

Details of the SCUBA2 data and the full maps and analysis are presented in C. Ross et al. (in prep).

0.2.3 SMA 870μm mosaic of core region

The SCUBA2 map has highlighted an apparent overdensity of 850um continuum blended in the core region. Large variations in CO(3-2) line luminosity to gas mass and dust mass mean that we cannot reliably use the detected CO sources to deconvolve the 850um emission. We thus embarked on an SMA survey to resolve the core region of the protocluster at 870um effective wavelength. The SMA map shown in Fig. A1 has resolved the SCUBA2 emission into at least 6 sources.

Describe SMA survey. Details of the SMA data in C. Ross et al. (in prep)

DISCUSSION OF OVERDENSITY WITH RADIUS, SMA DATA, VS S2 DATA

It is of interest to explore how concentrated this core is relative to the outer regions of the

protocluster.

0.3 Line detection significance and statistics

0.3.1 Blind line detection.

chance of finding lines associated and unassociated to UV galaxies

0.3.2 Stacking on UV galaxies.

3sigma detection once removing all those with $> 4sigma$ lines. Rob to verify with his code.

0.3.3 Chance probabilities and monte carlo experiment.

measured spectra in random positions, finding no lines.

0.4 Individual CO(3-2) line properties

Through our many new CO(3-2) detections in these fields, we study the bulk CO width (halo dynamics), the offset from optical lines (winds), and the potential for internal blue-red offset measurements (kinematics), comparing to the handfuls of CO(3-2) measurements of SMGs and lensed LBGs in the literature (e.g., Riechers et al. 2010).

Fig. 1. SMA 870μm mosaic map (40″ by 30″) of the z∼2.84 H1549 protocluster field. CO-emitters from the PdBI map are shown as blue circles, while the SCUBA2 contours are shown overlaid (white). The SMA has effectively detected at least 5 of the CO emitters at 870μm continuum, clearly explaining the unresolved SCUBA2 emission, and allowing for far-IR SEDs to be fit to individual CO-emitting galaxies, and gas/dust ratios to be estimated precisely. These observations constrain the ISM properties and elucidate the effect of the large overdensity on the gas supplies, stellar masses, and star formation modes relative to the field population.